

Proceeding Paper

Study of Beeswax–Carbon Nanotubes–Paperboard Nanocomposite for Temperature Regulation of Packaging Container †

Tejashree Amberkar *  and Prakash Mahanwar

Department of Polymer and Surface Engineering, Institute of Chemical Technology, Mumbai 400019, India; pa.mahanawar@ictmumbai.edu.in

* Correspondence: tejuamberkar@yahoo.co.in

† Presented at the 3rd International Online Conference on Nanomaterials, 25 April–10 May 2022; Available online: <https://iocn2022.sciforum.net/>.

Abstract: Beeswax is a bio-based organic phase change material. It undergoes solid to liquid phase transition at 61 °C with the phase transition enthalpy of 216 J/g. The high thermal energy storage enthalpy of beeswax is suitable for maintaining a constant temperature. However, the low thermal conductivity of beeswax limits the heat transfer rate. Furthermore, beeswax should be form-stabilized to minimize leakage in the molten state. In this study, the thermal conductivity of beeswax was improved with carbon nanotube (CNT) incorporation. The leakage of molten beeswax was minimized by coating it on paperboard. The beeswax–CNT–paperboard nanocomposite was further coated with silicone adhesive. It ensured the retention of molten wax. FTIR spectrum and SEM morphology analysis of the nanocomposites confirmed the physical dispersion of CNTs into the matrix. DSC analysis of nanocomposites showed a reduction of TES enthalpy to 98.52 J/g.

Keywords: phase change material; thermal energy storage; carbon nanotubes; beeswax; latent heat



Citation: Amberkar, T.; Mahanwar, P. Study of Beeswax–Carbon Nanotubes–Paperboard Nanocomposite for Temperature Regulation of Packaging Container. *Mater. Proc.* **2022**, *9*, 9. <https://doi.org/10.3390/materproc2022009009>

Academic Editor: Guanying Chen

Published: 29 April 2022

Publisher's Note: MDPI stays neutral with regard to jurisdictional claims in published maps and institutional affiliations.



Copyright: © 2022 by the authors. Licensee MDPI, Basel, Switzerland. This article is an open access article distributed under the terms and conditions of the Creative Commons Attribution (CC BY) license (<https://creativecommons.org/licenses/by/4.0/>).

1. Introduction

Organic phase change materials (PCMs) have low thermal conductivity [1]. The low thermal conductivity of PCM lowers the speed of heat conduction. Many researchers have used different strategies for improving the heat conductivity of PCM. The low thermal conductivity of PCM has been improved with various carbon-based and metal-based nanomaterials [2]. The inclusion of nanomaterials improves the thermal conductivity of synthesized nanocomposites. However, it also changes the density, chemical and mechanical properties of the composite. The carbon-based nanomaterials have a density near $2.26 \text{ g}\cdot\text{cm}^{-3}$ which is much lower than metal-based nanomaterials [3]. Dispersing dense metal nanoparticles uniformly in a matrix is a challenging task. Non-uniform dispersion gives anisotropic thermal properties. The carbon-based nanomaterials are more stable to chemical and thermal treatments. Such processes are often involved in form stabilization of PCM. Thus, carbon-based nanomaterials are preferred over metal-based nanomaterials for improving the thermal conductivity of organic PCMs.

The carbon-based nanomaterials come in different morphologies [4]. The morphology affects the aspect ratio, percolation and heat transfer route in the composite. Tao, Lin and He studied the thermal properties of carbon-based nanocomposites with four morphologies [5]. Fullerene C_{60} possesses spherical morphology. The spherical fullerene structure lowered thermal conductivity in the nanocomposite. The geometry of graphene nanoplatelets can be described as a 2D-square sheet. Graphene nanocomposites had comparatively lower heat storage enthalpy. The single-walled carbon nanotubes (SWCNT) and the multi-walled carbon nanotubes (MWCNT) have short cylindrical and long cylindrical morphology, respectively. Out of all nanocomposites, CNT nanocomposites showed the highest increase

in thermal conductivity. This structure helps in hindering leakage of molten beeswax. The thermal conductivity values were slightly higher for SWCNT composites. Considering the cost factor of preparing SWCNTs and MWCNTs, MWCNT nanocomposites are suitable for practical applications. The nanocomposites require an additional container to achieve a customized shape for application. Polymeric materials serve as a good matrix for PCM–CNT nanocomposites. Ma et al. [6] used bottlebrush crystalline silicon polymers for incorporating paraffin wax and CNTs. This polymeric matrix added material-specific properties suitable for the application. The 3D polymer network is flexible and superhydrophobic. The presence of CNTs improved the thermal conductivity of the composite. Such multifunctional composite finds application in wearable devices, electronic machines, building materials, etc.

Beeswax (BW) is an eco-friendly PCM. The low carbon footprint associated with BW production makes it a promising candidate for thermal energy storage (TES) applications. Its phase transition temperature is suitable for food packaging applications [7,8]. The use of thermal energy storing beeswax–paperboard sheets inside insulated packaging containers helps in maintaining the desired temperature for a longer time. However, beeswax is an organic PCM with low thermal conductivity of $0.25\text{--}0.3\text{ W}\cdot\text{m}^{-1}\cdot\text{K}^{-1}$ [9,10]. In this study, BW–MWCNT nanocomposite is prepared for improving the thermal performance of packaging containers. The high thermal conductivity and low density of MWCNTs are suitable for dispersing CNTs in the BW matrix. BW–CNT nanocomposite will possess high thermal conductivity helping in improving the heat transfer rate. BW–CNT nanocomposite can be coated on paper sheets of the required shape in the packaging application. The thermal performance of BW–CNT–paperboard composite sheet was studied in an insulated packaging container.

2. Materials and Methods

2.1. Materials

Beeswax was procured from anaha™, Goa, India. MWCNTs with a diameter of 30–50 nm and length of 10–30 μm were purchased from Sisco research laboratories Pvt. Ltd., Mumbai, India. Commercially available uncoated paper sheets were obtained from the local market in Mumbai, India. Tween 80 was obtained from SD fine chemicals private limited, Mumbai, India. Room temperature vulcanizing silicone adhesive was purchased from Astral adhesives, Gujrat, India. Sodium benzoate was purchased from Shree Lakshmi chemicals, Bangalore, India. For the experiments, DI water was used. Arduino UNO, Adiy™, Mumbai, India, was used to build and program the temperature data logger. An expanded polystyrene insulation sheet, two bigger cartons ($1 \times 13 \times 25\text{ cm}^3$) and two smaller cartons ($16 \times 10 \times 22.5\text{ cm}^3$) were purchased from a local market in Mumbai, India.

2.2. Method of Preparation

The suspension of CNT in DI water was prepared with two drops of emulsifier by ultrasonication for 1 h. The BW–CNT composites were made by adding suspension into a mixture of molten beeswax, one weight percent emulsifier, and two weight percent antimicrobial agent. The nanocomposites with CNT concentrations of 0.02 wt.%, 0.04 wt.%, 0.06 wt.% and 0.08 wt.% were prepared. The prepared solution was heated at $70\text{ }^\circ\text{C}$ for 30 min under magnetic stirring in a closed container. The water was evaporated from the solution at $100\text{ }^\circ\text{C}$. The mixture was again homogenized at $70\text{ }^\circ\text{C}$ for 30 min under ultrasonication. The molten mixture was coated on paper sheets. The papers were dried at room temperature (RT). The silicon adhesive coat was applied after 24 h. The prepared sheets were further dried for seven days.

2.3. Characterization Techniques

2.3.1. T-History

The setup consisted of two identical test tubes with water as reference material and sample PCM nanocomposite. The test tubes were heated to 70 °C and their cooling process at RT was recorded with temperature sensors. The temperature–time graph of the reference and BW–CNT composite were plotted with obtained data.

The specific heat, heat of fusion and thermal conductivity of the BW–CNT composite are determined using the following formula [11]

$$c_p = \frac{m_R * c_{p,R} + m_t * c_{p,t}}{m_p} \times \frac{A_3}{A_2'} - \frac{m_t * c_{p,t}}{m_p}$$

where m_R is the mass of reference material, m_t is the mass of tube material, m_p is the mass of BW–CNT composite, c_p is the specific heat capacity of the BW–CNT composite sample, $c_{p,R}$ is the specific heat capacity of the reference material, $c_{p,t}$ is the specific heat capacity of the tube material, A_3 is the area under the cooling curve of the BW–CNT composite and A_2' is the area under the cooling curve reference material as shown in Figure 1.

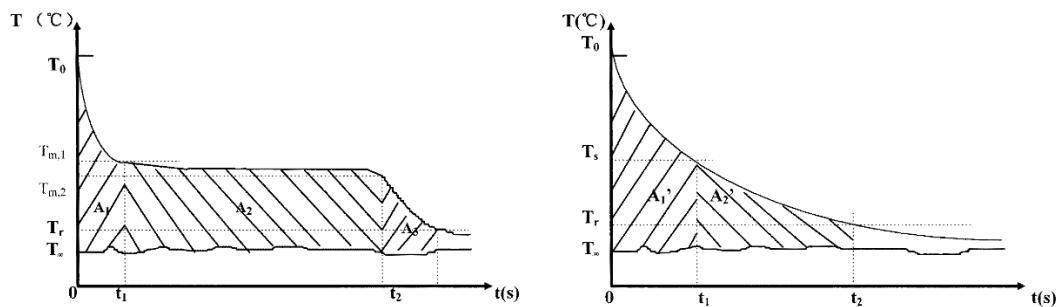


Figure 1. Illustration of T-history curve of PCM (left) and water (right). Adapted with permission from Ref. [12]. Copyright 1999 Institute of Physics (Great Britain).

The heat of fusion can be calculated using the formula [12]:

$$H_m = \frac{m_R * c_{p,R} + m_t * c_{p,t}}{m_p} \times \frac{A_2}{A_1'} (T_0 - T_{m,1}) - \frac{m_t * c_{p,t}}{m_p} (T_{m,1} - T_{m,2})$$

where m_R is the mass of reference material, m_t is the mass of tube material, m_p is the mass of BW–CNT composite, c_p is the specific heat capacity of the BW–CNT composite sample, $c_{p,R}$ is the specific heat capacity of the reference material, $c_{p,t}$ is the specific heat capacity of the tube material, T_0 is the temperature at the start of the experiment, $T_{m,1}$ is the temperature at the start of the phase transition process of the BW–CNT composite, $T_{m,2}$ is the temperature at the end of the phase transition process of the BW–CNT composite, T_R is the reference temperature, A_2 is the area under the cooling curve of BW–CNT composite and A_1' is the area under the cooling curve reference material as shown in Figure 1.

The thermal conductivity of the BW–CNT composite was calculated using the formula [11]:

$$k_p = \left[1 + \frac{c_p (T_m - T_\infty)}{H_m} \right] / 4 \left[\frac{t_f (T_m - T_\infty)}{R^2 \rho_p H_m} \right]$$

where k_p is the effective thermal conductivity of the BW–CNT composite, c_p is the specific heat of the BW–CNT composite, ρ_p is the density of the BW–CNT composite, R is the radius of the test tube, H_m is the heat of fusion of the BW–CNT composite as obtained from the DSC results and T_m and T_∞ are the temperatures of melting and atmosphere, respectively. Time of solidification of the molten BW–CNT composite is denoted by t_f .

2.3.2. Scanning Electron Microscopy

The scanning electron microscope (SEM) was used to examine the morphology of the nanocomposites. The morphology of BW–CNT composite and coated BW–CNT–paperboard composite samples was studied using FEI Quanta 200 SEM model.

2.3.3. Leakage Test

The circular sheets of coated and uncoated BW–CNT–paperboard composite samples were heated to 70 °C on the white sheet for 15 mins. The leakage was observed visually on the white sheet after removing the samples. The effectivity of coating in form-stabilizing beeswax can be examined with this leakage test.

2.3.4. Fourier Transform Infrared Spectroscopy

The BW–CNT composite samples were scanned in the Fourier Transform Infrared (FTIR) spectroscope in the 4000–500 cm^{-1} range using a Bruker Alpha spectrometer in attenuated total reflectance spectra mode.

2.3.5. Differential Scanning Calorimetry

The differential scanning calorimeter (DSC) DSC 3, Mettler Toledo, Tokyo was used to analyze the thermal properties of the BW–CNT composite in the temperature range of 25 °C to 100 °C. The heating rate of 10 °C/min was achieved in a nitrogen atmosphere.

2.3.6. Heat Release Performance in Carton

The heat release performance of prepared nanocomposite sheets was checked with an assembly depicted in the published paper [8]. The thermal performance of the empty control sample and filled BW–CNT–paperboard composite sheet sample was studied. The glasses of boiled water were placed in smaller cartons and consequently in larger cartons as shown in Figure 2. The empty space between the smaller and larger carton walls was filled with polystyrene insulation sheets and 60 g BW–CNT–paperboard nanocomposite sheets. The drop in temperature of the water was measured with a data logger.

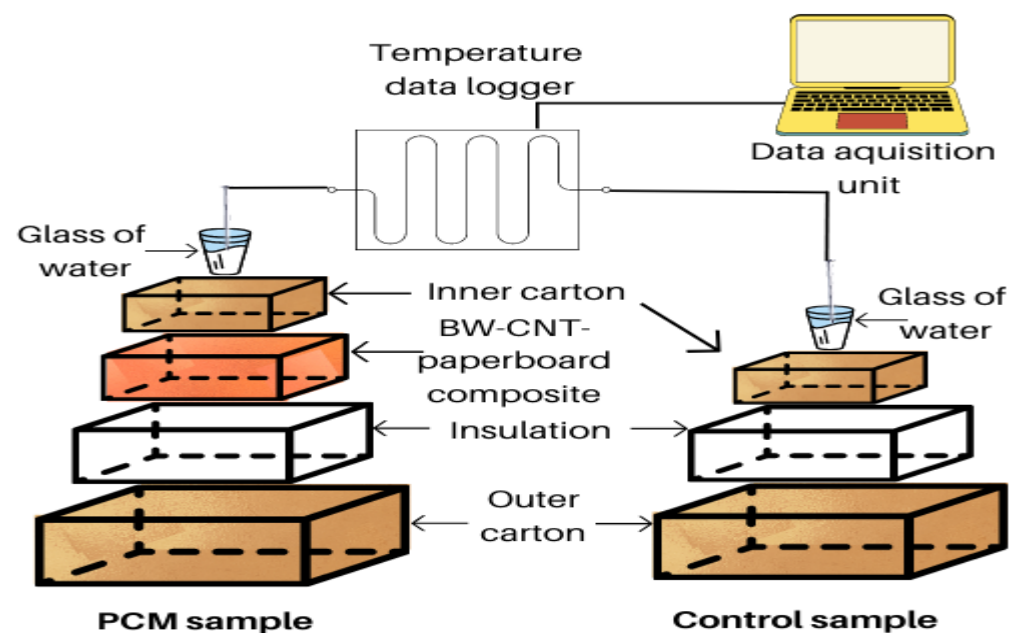


Figure 2. Assembly for heat release performance testing [8].

3. Results and Discussion

The T-history method performed on BW and BW–CNT composites gave temperature–time profiles which are shown in Figure 3. The presence of CNTs modified the temperature–time profiles. The values H_m , thermal conductivity and time of phase transition calculated from these profiles are shown in Table 1. The thermally conductive CNTs form conductive path networks for faster heat transfer in BW composite structures. With 0.02% addition in CNT concentration, phase transition time decreased by 5.08% 11.53% 13.78% and 15.93%, respectively. This reduction was smaller for BW-0.06 CNT and BW-0.08 CNT composites. The thermal conductivity of BW–CNT composites increases with an increase in CNT concentration. The values can be observed in Table 1. This increase was less for 0.06% and 0.08% CNT concentration. A possible reason for these anomalous values could be the agglomeration of CNTs. The enthalpy of the crystalline structure of beeswax reduced slightly with the presence of CNTs. An increase in CNT concentration decreases the H_m value by a small amount. This change is within 3% of pure beeswax enthalpy.

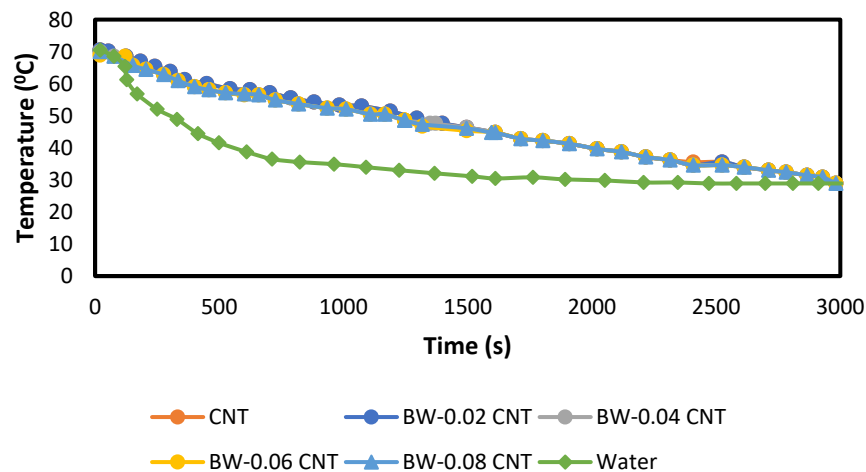


Figure 3. Temperature–time profiles of BW and BW–CNT composites.

Table 1. T-history test results.

Composition	Time of Phase Transition (s)	Decrease in Time of Phase Transition (%)	Thermal Conductivity ($W \cdot m^{-1} \cdot K^{-1}$)	Increase in Thermal Conductivity (%)	H_m (J/g)
BW	1023	0	0.284	0	220.71
BW-0.02 CNT	971	5.08	0.298	4.92	220
BW-0.04 CNT	905	11.53	0.308	8.45	217.72
BW-0.06 CNT	882	13.78	0.312	9.86	215.92
BW-0.08 CNT	860	15.93	0.315	10.91	214.55

SEM analysis of the BW-0.04 CNT and BW-0.06 CNT composites is represented in Figure 4. The BW-0.04 CNT composite showed uniform dispersion. The agglomerates found in BW-0.06 CNT composite sample showed entanglement of CNTs at higher magnification.

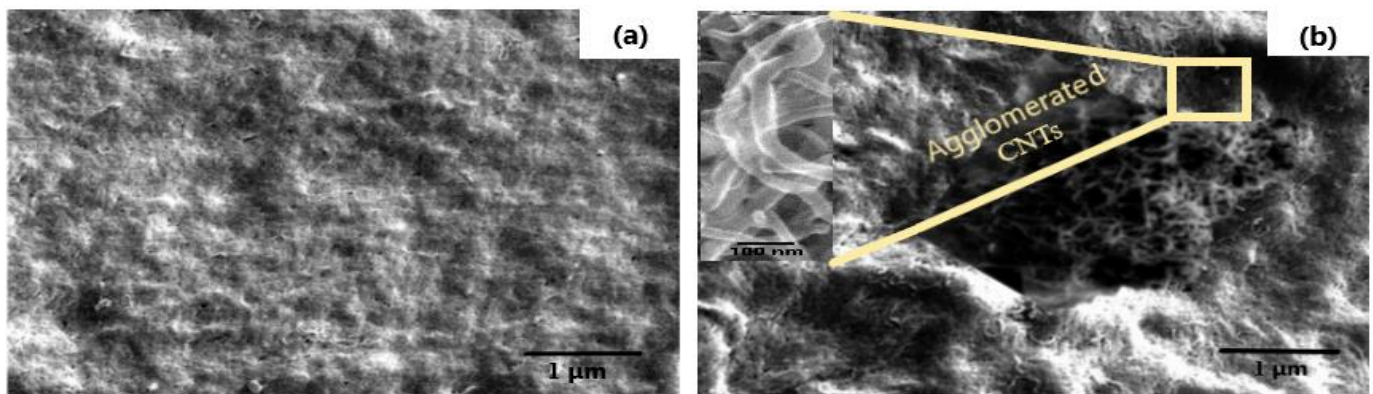


Figure 4. Morphology of (a) BW-0.04 CNT and (b) BW-0.06 CNT.

SEM analysis of the coated BW-0.04 CNT–paperboard and BW-0.06 CNT–paperboard composites is represented in Figure 5. Smooth morphology is observed in Figure 5a. The spots in Figure 5b might be due to CNTs agglomeration. The surfactant concentration was not sufficient to disperse CNTs in the BW-0.06 composite. The agglomeration of CNTs creates a non-uniform heat transfer network in the composite. Thus, the thermal properties of BW-0.06 CNT and BW-0.08 CNT did not improve significantly. The BW-0.04 CNT composite has good heat storage enthalpy and high thermal conductivity. It was selected for improving the thermal performance of packaging containers.

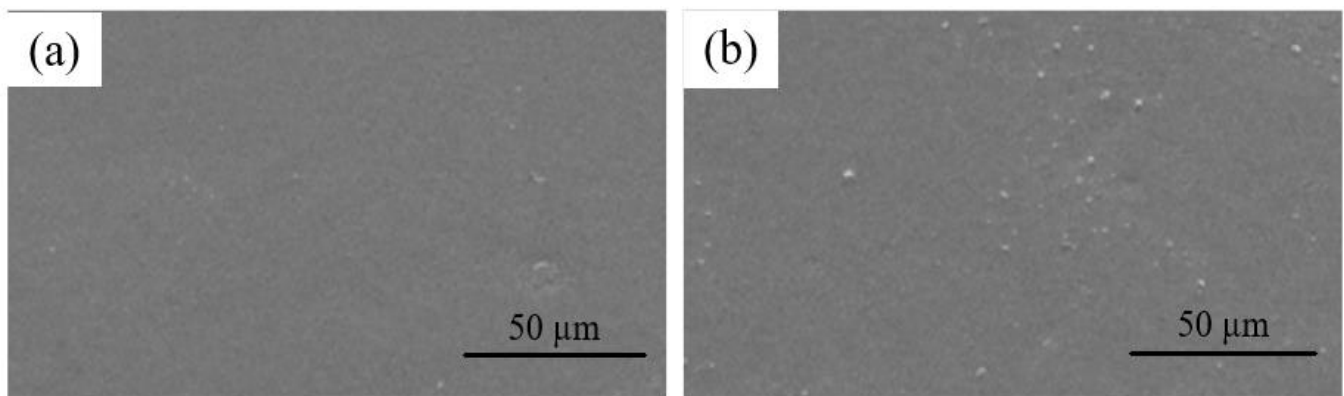


Figure 5. Morphology of coated (a) BW-0.04 CNT–paperboard composite and (b) BW-0.06 CNT–paperboard composite.

The leakage test examines the effectivity of silicon coating in hindering leakage of molten beeswax. As shown in Figure 6, the uncoated sample showed leakage at 70 °C. The molten BW oozed out of BW–CNT composite coating. On the other hand, the coated sample did not show leakage. The protective silicone coating layer on the nanocomposite coating prevented leakage of molten beeswax. It improves the form-stability of nanocomposite coating. Form-stable BW–CNT coating can provide TES for a longer time since the content of beeswax is protected from leaking away.

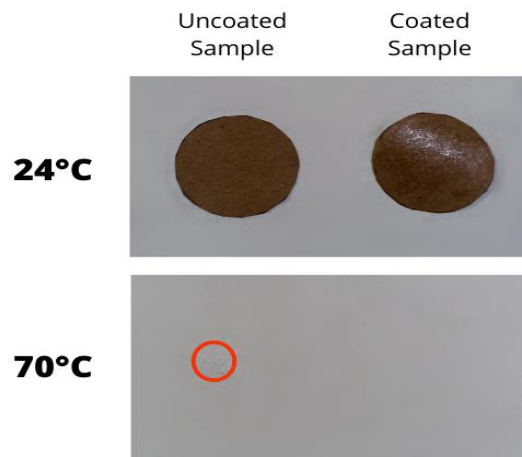


Figure 6. Leakage test.

Beeswax's FTIR spectrum shown in Figure 7a reveals the chemical structures of its constituents. The peak at 719 cm^{-1} corresponds to rocking vibrations of long-chain hydrocarbons (HCs). The C–O stretching arising from the aromatic ester is represented by the band at 1365 cm^{-1} . The C–H bending of aliphatic HCs is responsible for the peak at 1463 cm^{-1} . The band at 1691 cm^{-1} represented stretching vibrations emanating from the C=O bond in aromatic acid. The peak at 1103 represents vibrations of the C–O bond in the ester group. The peaks at 2846 cm^{-1} and 2920 cm^{-1} arise from stretching vibrations of the CH_2 group. The BW-0.04 CNT spectrum in Figure 7b contained all the typical peaks of beeswax. No new peaks were observed. This confirms the physical dispersion of CNTs into the beeswax matrix.

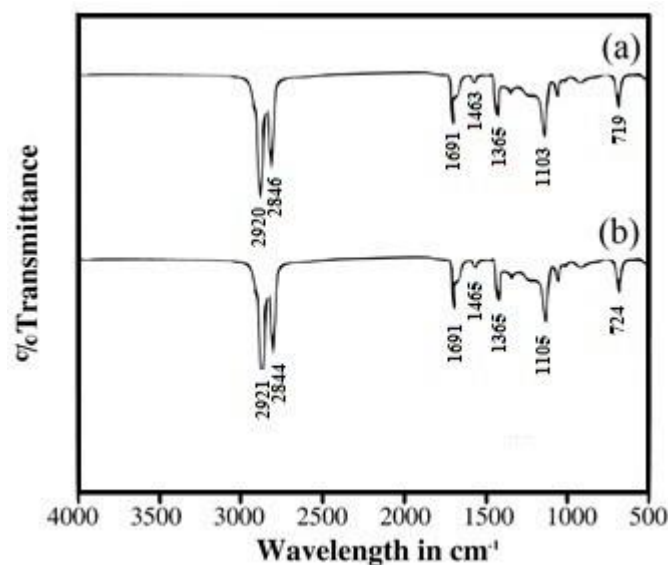


Figure 7. FTIR spectra of (a) BW and (b) BW-0.04 CNT.

The heat release test was used to investigate the effectivity of coated BW-0.04 CNT–paperboard nanocomposite sheets on the temperature of confined water. The temperature–time curve of water in the PCM nanocomposite sheet sample and the control sample carton is shown in Figure 8. Temperature measurements were taken at the same time for both samples. Temperature measurements for the samples began at $88\text{ }^\circ\text{C}$. Initially, for 1872 s , the PCM nanocomposite sample and control sample reduced the temperature of water to around $62\text{ }^\circ\text{C}$ with a similar temperature–time profile. At 4031 s , the water in the control assembly reached ambient temperature. It took less time for the control assembly to attain

ambient temperature. The heat storage enthalpy of BW and BW-0.04 CNT composite was 216.09 J/g and 98.52 J/g, respectively, in DSC. The TES phenomenon of PCM is confirmed by the increase in time to attain ambient temperature for PCM nanocomposite sheets. The interior temperature remained higher for longer in the composite assembly than in the control assembly. The heat transfer from the PCM to the interior chamber is responsible for the increased temperature inside the carton. In the event of a delayed supply, this phenomenon can be employed to maintain a greater temperature.

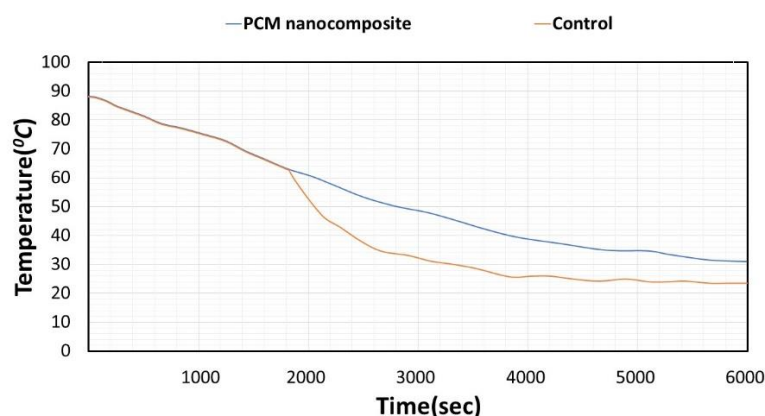


Figure 8. Temperature–time profile of control sample and PCM nanocomposite sample.

4. Conclusions

T-history analysis showed thermal conductivity and heat storage enthalpy of BW–0.04 CNT composite as $0.308 \text{ W} \cdot \text{m}^{-1} \cdot \text{K}^{-1}$ and 217.72 J/g , respectively. The CNT concentration of 0.04% showed good dispersion in beeswax in SEM analysis. Physical mixing of PCM and CNT was confirmed by FTIR. DSC examination of the BW-0.04 CNT paper composite revealed good heat storage capabilities with melting enthalpy of 98.52 J/g . The use of PCM nanocomposite sheets can lengthen the time it takes to maintain food temperature close to the composite’s phase transition temperature.

Author Contributions: Writing—original draft preparation, T.A.; writing—review and editing, P.M. All authors have read and agreed to the published version of the manuscript.

Funding: This work is funded by AICTE National Doctoral Fellowship Scheme sanctioned vide letter F No: 12-2/2019-U1 provided by the Ministry of Human Resource Development, Government of India.

Institutional Review Board Statement: Not applicable.

Informed Consent Statement: Not applicable.

Data Availability Statement: The data presented in this study are available on request from the corresponding author.

Acknowledgments: The authors acknowledge research facilities provided by the Institute of Chemical Technology, Mumbai.

Conflicts of Interest: The authors declare no conflict of interest.

References

1. Pielichowska, K.; Pielichowski, K. Phase change materials for thermal energy storage. *Prog. Mater. Sci.* **2014**, *65*, 67–123. [[CrossRef](#)]
2. Lin, Y.; Jia, Y.; Alva, G.; Fang, G. Review on thermal conductivity enhancement, thermal properties and applications of phase change materials in thermal energy storage. *Renew. Sustain. Energy Rev.* **2018**, *82*, 2730–2742. [[CrossRef](#)]
3. Zhang, Q.; Luo, Z.; Guo, Q.; Wu, G. Preparation and thermal properties of short carbon fibers/erythritol phase change materials. *Energy Convers. Manag.* **2017**, *136*, 220–228. [[CrossRef](#)]
4. Huang, X.; Alva, G.; Jia, Y.; Fang, G. Morphological characterization and applications of phase change materials in thermal energy storage: A review. *Renew. Sustain. Energy Rev.* **2017**, *72*, 128–145. [[CrossRef](#)]

5. Tao, Y.B.; Lin, C.H.; He, Y.L. Preparation and thermal properties characterization of carbonate salt/carbon nanomaterial composite phase change material. *Energy Convers. Manag.* **2015**, *97*, 103–110. [[CrossRef](#)]
6. Ma, J.; Ma, T.; Duan, W.; Wang, W.; Cheng, J.; Zhang, J. Superhydrophobic, multi-responsive and flexible bottlebrush-network-based form-stable phase change materials for thermal energy storage and sprayable coatings. *J. Mater. Chem. A* **2020**, *8*, 22315–22326. [[CrossRef](#)]
7. Amberkar, T.; Mahanwar, P. Composite Phase Change Material for Improving Thermal Protection Performance of Insulated Packaging Container. *Int. J. Eng. Trends Technol.* **2022**, *70*, 59–64. [[CrossRef](#)]
8. Amberkar, T.; Mahanwar, P. Study and Characterization of Phase Change Material-Recycled Paperboard Composite for Thermoregulated Packaging Applications. *Mater. Proc.* **2021**, *7*, 17. [[CrossRef](#)]
9. Amin, M.; Putra, N.; Kosasih, E.A.; Prawiro, E.; Luanto, R.A.; Mahlia, T.M.I. Thermal properties of beeswax/graphene phase change material as energy storage for building applications. *Appl. Therm. Eng.* **2017**, *112*, 273–280. [[CrossRef](#)]
10. Mishra, D.K.; Bhowmik, S.; Pandey, K.M.; Hui, W. Analysis of Heat Transfer Rate for Different Annulus Shape Properties-Enhanced Beeswax-Based Phase Change Material for Thermal Energy Storage. *Math. Probl. Eng.* **2022**, *2022*, 3472. [[CrossRef](#)]
11. Venkataraj, K.P.; Suresh, S.; Praveen, B.; Arjun, V.; Sreeju, C. Pentaerythritol with alumina nano additives for thermal energy storage applications. *J. Energy Storage* **2017**, *13*, 359–377. [[CrossRef](#)]
12. Yinping, Z.; Yi, J.; Yi, J. A simple method, the T-history method, of determining the heat of fusion, specific heat and thermal conductivity of phase-change materials. *Meas. Sci. Technol.* **1999**, *10*, 201–205. [[CrossRef](#)]